Chinese Journal of Aeronautics, (2015), 28(3): 712–719

Chinese Society of Aeronautics and Astronautics
& Beihang University

Chinese Journal of Aeronautics

cja@buaa.edu.cn
www.sciencedirect.com

A novel environmental control system based on membrane dehumidification

Yuan Weixing [a,*], Yang Bo [a], Guo Binghan [a], Li Xiangping [b], Zuo Yansheng [b], Hu Wenchao [b]

[a] *Laboratory of Ergonomics and Environmental Control, School of Aeronautic Science and Engineering, Beihang University, Beijing 100191, China*
[b] *Jincheng Electromechanical Center of Nanjing, Nanjing 211102, China*

Received 10 October 2014; revised 17 March 2015; accepted 30 March 2015
Available online 20 April 2015

KEYWORDS

Aircraft;
Cooling performance;
Environmental control system;
High pressure de-water;
Membrane dehumidification;
Sweep ratio

Abstract This paper conducts a simulation study of a novel aircraft environmental control system based on membrane dehumidification (MD-ECS), and compares the system with the up-to-date four-wheel high pressure de-water system (4WHPDW-ECS). Mathematical models for the two systems are established, and a system simulation using a numerical technique is performed to analyze and compare the cooling performance of the two systems. Simulation results show that the cooling capacity of MD-ECS is much higher than that of 4WHPDW-ECS under the same working conditions, indicating that the novel system is theoretically feasible and promising. The effects of the sweep ratio of the membrane dehumidifier on the dehumidification and cooling performance of the system is also investigated.

1. Introduction

Vapor compression refrigeration (VCR) is the most common cooling technology widely applied in heating, ventilation and air conditioning (HVAC), ice making, food storage, etc. However, its performance strongly depends on ambient conditions, and the vapor compressor may become the main drawback because of the oil scavenging problem in some severely moving circumstances such as ships, high speed trains and aircrafts. In contrast, air cycle derived from inverse Brayton cycle has been developed as the main cooling technology in aircrafts after the earliest application in the fighter during 1940s, with the advantages of light weight, few components and easy maintenance. In particular, air cycle consumes almost no electric power, and is proved to be the best cooling technology before the development of all-electric aircraft (AEA).

With the development of wide-bodied airliners and rapid increase of the power of the avionics equipments, the basic air cycle system mainly consisting of only an air compressor and a turbine[1,2] has to be modified gradually to meet the increasing demand of cooling capacity. It is found that the humidity drastically limits the cooling capacity. Especially on the ground or at low flight height where the ambient humidity

* Corresponding author. Tel.: +86 10 82338878.
E-mail address: yuanwx@buaa.edu.cn (W. Yuan).

Peer review under responsibility of Editorial Committee of CJA.

ELSEVIER Production and hosting by Elsevier

http://dx.doi.org/10.1016/j.cja.2015.04.016

is relatively high, the refrigeration temperature cannot be too low, otherwise dewing and even freezing may take place at the turbine exit. Consequently, high pressure de-water (HPDW) system is currently widely applied.[3] Before entering the turbine, the pressurized humid air is cooled by a condenser and the condensate water droplets are then separated by a water separator. Compared with low pressure de-water (LPDW) system,[4,5] HPDW has many advantages including:[6] (A) the water vapor is condensed more easily due to higher dew point temperature at high pressure; (B) high pressure breeds high density and therefore low air velocity, so the condensate droplets are big enough to promote the separation efficiency, while the mist caused by high air velocity is hard to be removed in LPDW; (C) HPDW system can obtain significant cooling capacity by achieving low enough temperature at the turbine exit, free from freezing risk. Currently, the most advanced environmental control system (ECS) is the four-wheel type (4WHPDW-ECS) system consisting of a compressor, a fan (sometimes replaced by another compressor to further increase the pressure) and two turbines, which has been applied in B777 and A380 airliners. In such a system, the water vapor is condensed in the condenser by the cold dry air discharged from the primary turbine and is then removed by the water separator. Finally, the cold dry air enters the secondary turbine for further expansion to obtain even lower temperature. The primary turbine achieves a low refrigeration temperature above the ice point of the airflow, so the possibility of condenser freezing is eliminated. Therefore, the 4WHPDW-ECS system is superior to three-wheel system which has only one big turbine.[3,7,8] Moreover, two-stage low-intensity expansions reduce the turbine energy loss, compared with one-stage high-intensity expansion within the same overall expansion ratio.

However, the 4WHPDW-ECS also has disadvantages including higher weight and more complex structure in comparison with former ECS types. The water vapor removal fundamental hardly changes from LPDW to HPDW, as water vapor removal is achieved by successive condensation and mechanical separation. The de-water systems have to consume much cooling capacity of turbine(s) to lower the air temperature below the dew point. Totally different from the conventional water vapor removal method, a novel environmental control system based on membrane dehumidification is proposed in this study to replace the group of the condenser and water separator[9] used in HPDW-ECS. In this novel system, the water vapor transfers across membranes from the high pressure feed air to the low pressure purging air without phase change. Therefore, the latent cooling capacity is totally reserved, and the cooling capacity supplied to the cabin is greatly promoted.

2. System description

2.1. Four-wheel high pressure de-water ECS

The schematic process of a typical 4WHPDW system is depicted in Fig. 1, the bleed air of high temperature and pressure is first cooled by the primary heat exchanger HX1, and is then further pressurized by the compressor, which also causes a temperature rise. After being compressed, it is further cooled by the secondary heat exchanger HX2. The ram air at low temperature flows at the cold sides of HX1 and HX2, propelled by the fan. It has been known that the high pressure air can be cooled remarkably through expansion. To prevent it from freezing, in the 4WHPDW-ECS, the bleed air is pretreated by a de-water process before entering the turbine. A condenser and a water separator are arranged before the primary turbine to remove the water vapor from the high pressure bleed air, where the cold source for condensation is the cold and dry air exhausted from the primary turbine. The latent heat is recycled by spraying the condensed water to the ram air side of HX2. A heat recuperator is used to increase the bleed air temperature properly to reduce the freezing risk during the following expansions. Then the cold and dry air flows across the cold side of the condenser and is cooled by the secondary turbine successively. Having met the supply air quality requirements, the product dry air is finally supplied to the cabin. Four rotary devices including the fan, the compressor and two turbines are coaxial with a power adaption and allocation mechanism, which is the reason for the naming of "four-wheel" system.

Compared with the traditional ECS, the 4WHPDW-ECS achieves a greater cooling capacity by utilizing high pressure de-water process, and the two-stage expansion reduces the possibility of freezing and turbine efficiency loss. Various heat recovery procedures, including pre-cooling by HX1 and HX2, heat recuperator and water spraying, promote the heat transfer efficiency of the whole system.

2.2. Membrane dehumidification ECS

However, the complexity of the 4WHPDW-ECS, as well as higher weight than that of the traditional systems, confines its application regardless of its advanced performance. To overcome these drawbacks, an original membrane dehumidification environmental control system (MD-ECS) is proposed, using a "shell-and-tube" type hollow fiber membrane dehumidifier to replace the metal-made group of the condenser and water separator. The schematic flowchart of the MD-ECS is shown in Fig. 2. With the same flow procedure before expansion as the 4WHPDW-ECS, the bleed air is propelled into the feed side (tube side) of the membrane dehumidifier, and is dehumidified by a certain ratio of the dry product air sweeping back in the permeate side (shell side). Since the outlet pressure of the feed side is still relatively high, this paper proposes a minor turbine for the sweep air before sweeping back, so as to obtain a greater trans-membrane water vapor partial pressure difference. The temperature of the sweep air decreases by expansion, so the dehumidification process is combined with a heat transfer process. After dehumidification, the sweep air is mixed with the ram air, flowing across the cold sides of HX1 and HX2. Apart from this proportion of sweep air, the remaining dry product air from the membrane dehumidifier is cooled down by expansion in the main turbine, and is supplied to the cabin finally.

In this novel system, the membrane dehumidifier is a key component. As a widely applied technology in the fields of separation and purification of compressed air and natural gas,[10,11] membrane dehumidification works on the principle of water vapor permeation under partial pressure difference across the microporous membrane, which is highly selective for water vapor with respect to dry air. Here, polyethersulfone (PES)

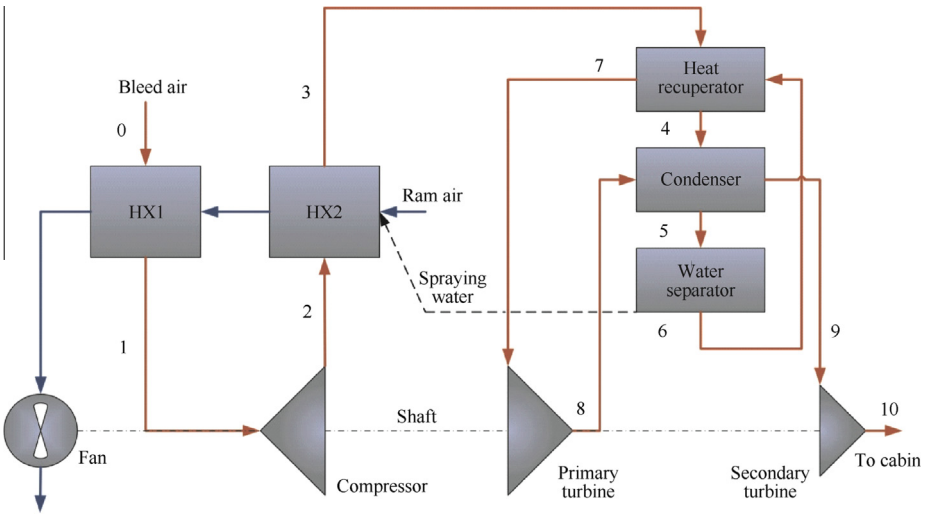

Fig. 1 Schematic of 4WHPDW-ECS.

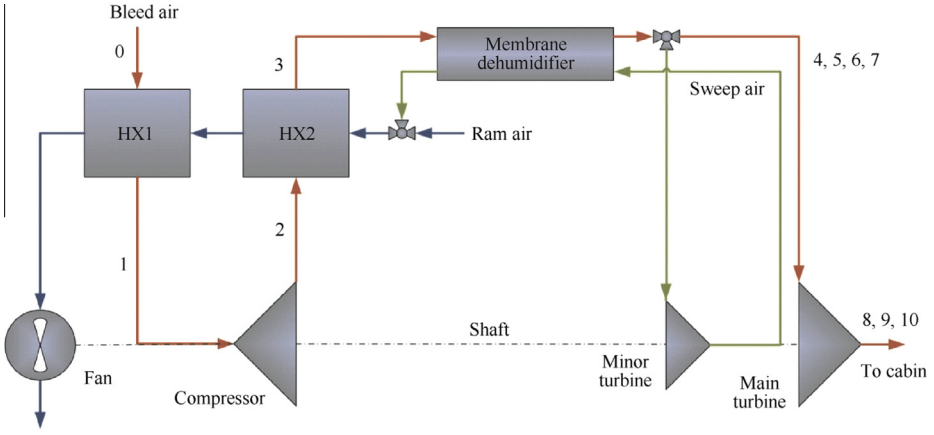

Fig. 2 Schematic of MD-ECS.

is chosen as the membrane material in the form of hollow fiber, which has excellent mechanical properties such as rigidity, wear-resistant and high strength, and can stand pressure as high as 1 MPa and temperature ranging from −100 to 150 °C.

Fig. 3 portraits the overview structure of a typical "shell-and-tube" type membrane dehumidifier. Thousands of hollow fibers are packed in the metal shell, with both terminations epoxy sealed to create tube-side chamber and shell-side chamber. The pressurized and humid air enters the membrane dehumidifier from entrance A and flows in the tube side (feed side). At the same time, the water vapor permeates from the tube side through the membrane pores towards the shell side (permeate side), and is swept away by the purging air whose flow rate can be adjusted by a valve installed aside purge gas inlet C. The product air in the tube side and the exhaust air in the shell side are discharged from exit B and discharge hole D, respectively.

3. Mathematical models and system simulation

3.1. Mathematical model for membrane dehumidifier

Since the models for the aircraft engine, turbine-compressor/fan, heat exchangers and simplified membrane dehumidifier have been introduced in our previous research,[9] this paper adopts a more detailed modeling for the membrane dehumidifier.

The permeation mechanisms of water vapor in membrane have been widely studied in literatures. Usually, the diffusion mechanism such as ordinary diffusion, Knudsen diffusion or the combination of them controls the water vapor flux under zero pressure difference. While under high pressure difference, Poiseuille flow (also called viscous flow) predominates the permeation process. Different from diffusion whose permeability is determined mainly by the structure properties of the membrane, Poiseuille flow permeability is affected remarkably by the mean pressure in pores as presented in:[12]

$$Pe = \frac{d_p^2 \varepsilon}{32\tau\delta} \cdot \frac{M_v p_m}{\mu R T_m} \tag{1}$$

where Pe is the permeability, d_p the pore diameter, ε the porosity, τ the tortuosity, δ the membrane thickness, M_v the molecular mass of water vapor, μ the dynamic viscosity of water vapor, R the ideal gas constant, 8.314 J/(mol·K), p_m and T_m are the mean pressure and temperature in pores, respectively. It can be seen that the right side of Eq. (1) consists of two parts. The left part outside the parenthesis reflects the

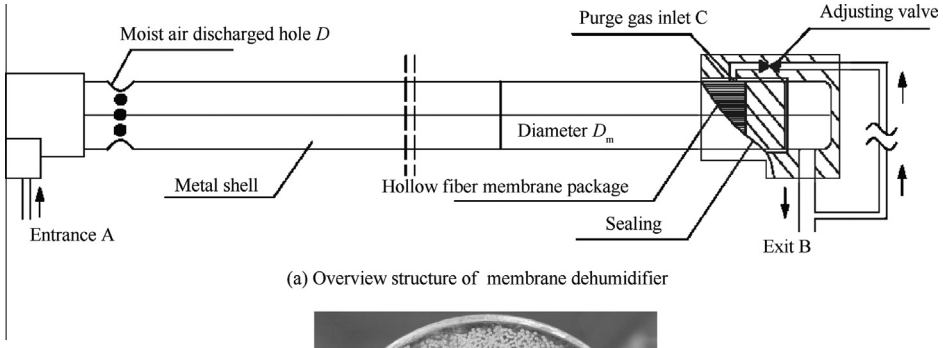

(a) Overview structure of membrane dehumidifier

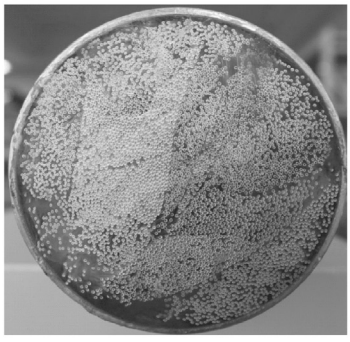

(b) Cross-section view of inlet termination

Fig. 3 Outline of the membrane dehumidifier.

membrane morphology similar to that in diffusion mechanism, while the right part in the parenthesis represents the thermodynamic properties of the water vapor in pores.

The mass flux through the membrane j_P is calculated by:

$$j_P = Pe(p_{v,i} - p_{v,o}) \tag{2}$$

where p_v is the water vapor partial pressure; the subscripts "i" and "o" represent the tube side and shell side, respectively.

Literatures have found that the flow velocity of either feed or permeate side can influence the permeation rate in high pressure air dehumidification.[10,13] In particular, when the flow velocity of the permeate side is low, the water molecules will concentrate on the membrane surface of the permeate side, which is called concentration polarization, and the mass transfer performance deteriorates therefore. It can be concluded that the diffusion mechanism also works. Under this mechanism, the water vapor flux is determined by the water vapor concentration (i.e., the water vapor density specified by the overall volume of the humid air) difference as below:

$$j_D = k_t(\rho_i\omega_i - \rho_o\omega_o) \tag{3}$$

where ρ is the air density, ω the humidity ratio; k_t is the total mass transfer coefficient on the basis of the outer surface area of the fibers, including the diffusion in membrane and the convective mass transfer in boundary layer at either side of the membrane as represented by:

$$\frac{1}{k_t} = \frac{1}{k_i}\left(\frac{d_o}{d_i}\right) + \frac{d_o}{2D_{vm}}\ln\left(\frac{d_o}{d_i}\right) + \frac{1}{k_o} \tag{4}$$

In this paper, it is considered that Knudsen diffusion dominates the diffusion process through membrane pores. Knudsen diffusivity can be calculated by:[14]

$$D_{vm} = \frac{d_p}{3}\sqrt{\frac{8RT_m}{\pi M_v}} \tag{5}$$

In recent years, some new convective mass transfer correlations have been developed for membrane process including h umidification/dehumidification, distillation, gas separation, bloody oxygenator, etc.[15–22] However, most of them are not applicable in our present study due to the different operating conditions or the complexity of those correlations. As a matter of fact, some traditional correlations are still widely used, by which the calculation accuracies are usually in the acceptable range. Here, the correlations for laminar flow by Lipnizki and Field are applied, as formulated by:[23]

$$Sh = (Sh_1^3 + Sh_2^3 + Sh_3^3)^{1/3} \tag{6}$$

$$Sh_1 = 3.66 + 1.2\phi^{-0.4} \tag{7}$$

$$Sh_2 = 1.615(1 + 0.14\phi)^3\left(\frac{ReScd_h}{L}\right)^{0.5} \tag{8}$$

$$Sh_3 = \left(\frac{2}{1 + 22Sc}\right)^{1/6}\left(\frac{ReScd_h}{L}\right)^{0.5} \tag{9}$$

where ϕ is the packing fraction of fibers in the shell, d_h the hydrodynamic diameter; L the fiber length; Re and Sc are the Reynolds number and the Schmidt number, respectively. When the Reynolds number exceeds 2300, the following equation is applied[23]:

$$Sh = 0.021\phi^{-0.225}Re^{0.8}Sc^{0.33} \tag{10}$$

The tube-side Sherwood number is calculated by:[24]

$$Sh = 1.62\left(\frac{ReScd_h}{L}\right)^{0.33} \tag{11}$$

The mass transfer coefficient can be calculated by the Sherwood number, as:

$$k = \frac{ShD_{va}}{d_h} \tag{12}$$

where D_{va} is the diffusivity of water vapor in air.

The overall mass flux is

$$j = j_P + j_D \tag{13}$$

Membrane dehumidification involves simultaneous heat and mass transfer. The following convective heat transfer correlations are applicable for both tube and shell sides in laminar and turbulent flow patterns, respectively:

$$Nu = 1.86\left(\frac{RePrd_h}{L}\right)^{0.33} \tag{14}$$

$$Nu = 0.023Re^{0.8}Pr^c \tag{15}$$

where c equals 0.4 when the fluid is heated and 0.3 when the fluid is cooled.

The friction coefficient f can be calculated by Blasius equations:

$$f = \begin{cases} 64/Re & Re < 2500 \\ 0.314Re^{-0.25} & 2500 < Re < 20000 \\ 0.184Re^{-0.2} & Re > 20000 \end{cases} \tag{16}$$

Then the pressure drop is obtained by:

$$dp = f\frac{\rho^2 u^2}{2d_h}dx \tag{17}$$

3.2. System simulation technique

In system simulation, each component of the system is taken as a module modeled with conversation equations. Inlet and outlet parameters are defined for each module, including mass flow rate, temperature, humidity ratio and pressure. The inlet parameters of one module are equal to the outlet parameters of the module upstream, whereby all the modules are connected and finally the system equations are established. There is a monotonic relation between the inlet and outlet parameters for each component, that is, an increase in the inlet value will cause an increase in the outlet value correspondingly, and vice versa. This means that the system is convergent, so the iterative calculation is applicable. The convergence residual is set as 1.0×10^{-5}.

4. Results and discussion

4.1. Dehumidification performance of membrane dehumidifier

The membrane dehumidifier is first numerically investigated by using finite differential scheme separately, in order to determine the proper working conditions and check whether the membrane dehumidifier is competent for the demands of the proposed ECS. The structural parameters of the membrane dehumidifier are listed in Table 1.

The effects of various working conditions on the dehumidification performance are calculated and analyzed. In this paper, dehumidification efficiency is chosen to evaluate the dehumidification performance. Given that the extreme outlet humidity ratio can reach zero for some special working conditions such as sufficient trans-membrane pressure difference, the dehumidification efficiency here is defined as follows:

$$\eta_{deh} = \frac{\omega_i - \omega_o}{\omega_i} \tag{18}$$

It has been known by calculation that the mass transfer resistance of the membrane is in the same order as or one order larger than that of either boundary layer, so the effect of the mass flow rate on the total mass transfer coefficient is quite limited under common working conditions. Instead, the dehumidification performance is determined by the partial pressure difference across the membrane, which is affected directly by the total pressure and the humidity ratio of both feed and permeate sides.

Fig. 4 shows the effects of the feed pressure on the dehumidification efficiency at different mass flow rates $\dot{m}_f$ of the feed air ranging from 0.10 kg/s to 0.30 kg/s, where the sweep ratio is fixed at 20%. It can be seen that the dehumidification efficiency increases along with the feed pressure. As the feed pressure increases further, the dehumidification efficiency increases more and more slowly and tends towards 1 in the end. Therefore, excessive feed pressure is not helpful to the promotion of dehumidification performance. Instead, too high pressure does harm to the structural strength. On the other hand, with fixed mass flow rate and sweep ratio, the feed pressure has a lower bound limit subject to the back pressure of the permeate side (see the "Limitation line" in Fig. 4). If the feed pressure is too low, after undergoing the tube-side pressure drop along the fibers, the inlet pressure of the sweep air may not provide enough driving force for sweeping in the given sweep ratio. Fig. 4 also shows the effects of the mass flow rate on dehumidification efficiency. The lower the mass flow rate is, the faster the humidity ratio drops, and the higher the dehumidification efficiency is. Additionally, at low flow rate, the tube-side pressure drop is low as well, so the airflow in the tube side is remained at relatively high total pressure, resulting in a greater mass transfer potential compared with that at high flow rate. Of course, the mass flow rate cannot be too low to satisfy the demand for the quantity of cabin air supply.

The effects of the sweep ratio are also studied, as shown in Fig. 5, where the feed pressure is fixed at 7×10^5 Pa with the feed air mass flow rates ranging from 0.10 kg/s to 0.30 kg/s. The humidity ratio of the sweep air increases slowly along the shell-side flow direction at high sweep ratio, obtaining a high average partial pressure difference. Therefore, the dehumidification performance is more excellent. Theoretically, the dehumidification efficiency can reach the maximum if all the feed air is swept back, with no air supplied to the cabin, however. Similar to the lower bound limit of the feed pressure described above, the sweep ratio has an upper bound limit determined by the feed pressure, as can be seen from the curve

Table 1 Parameters of the membrane dehumidifier.

Parameter	Value
Porosity ε	0.8
Tortuosity τ	3
Pore diameter d_p (nm)	15
Fiber outer diameter d_o (mm)	0.6
Membrane thickness δ (mm)	0.12
Fiber length L (mm)	650
Thermal conductivity λ (W/(m·K))	0.17
Shell inner diameter D (mm)	63
Fiber amount N	8000
Weight W (kg)	1.9
Volume V (cm^3)	4084

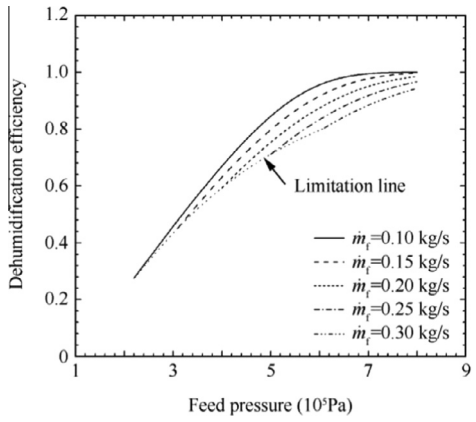

Fig. 4 Effects of feed pressure on dehumidification efficiency at various mass flow rates.

at 0.30 kg/s in Fig. 5, where the upper limits at other flow rates are not plotted for they are beyond the horizontal coordinate scale.

4.2. Comparisons of MD-ECS and 4WHPDW-ECS

It has been proven that the membrane dehumidifier proposed above is competent under the calculated working conditions in the section above, which are close to the system working conditions listed in Table 2.

All the nodes from 0 (system entrance) to 10 (system exit) of the two systems labeled in Figs. 1 and 2 are calculated and compared. The simulation results of key parameters including temperature, humidity ratio, enthalpy and pressure are plotted in Fig. 6. As can be seen in the figure, almost all the exit values of the parameters of the MD-ECS are lower than those of the 4WHPDW-ECS except that the exit pressure of the MD-ECS is slightly higher, indicating superior cooling and dehumidification performance of the MD-ECS. In the 4WHPDW-ECS, the exit temperature of the primary turbine (Node 8) is quite low, just slightly higher than that of MD-ECS. In the 4WHPDW-ECS, however, massive cooling capacity has to be consumed for condensation to remove water vapor in the primary air flow, with both temperature and enthalpy increasing from Node 8 to 9. The difference between enthalpy changes ($h_9 - h_8$) and ($h_4 - h_5$) is the latent heat of water vapor condensation. On the contrary, the water vapor removal is realized by "dry" process without occurrence of phase change in the membrane dehumidification, so that the cooling capacity is sufficiently reserved for cooling the air. Although the air mass flow rate is reduced by 20% for the reason of sweeping in the MD-ECS, the supply air reaches a temperature as low as 253.7 K, 25 K lower than that of the 4WHPDW-ECS. Besides, the humidity ratio of the supply air of the MD-ECS is lower than that of the 4WHPDW-ECS. Therefore, the total cooling capacity of the MD-ECS is still higher. For instance, with the same inlet conditions and required cabin air of 298 K and 30%RH, the cooling capacity of the MD-ECS can reach as high as 9.2 kW, while the cooling capacity of the 4WHPDW-ECS is only 5.4 kW. Here, the cooling capacity is defined by:

$$Q = G_s(h_c - h_s) \tag{19}$$

where G_s is the mass flow rate of supply air; h_c and h_s are the specific enthalpy of cabin air and supply air, respectively.

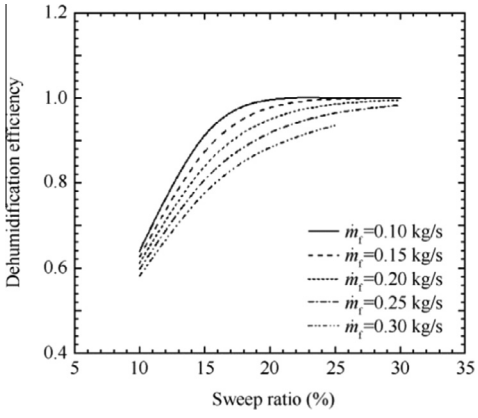

Fig. 5 Effects of sweep ratio on dehumidification efficiency at various mass flow rates.

4.3. Effects of sweep ratio on system performance of MD-ECS

The sweep ratio can be adjusted to regulate the system performance of the MD-ECS. The system applies a minor turbine to expand and cool the sweep air before it sweeps back. Hence, the sweep ratio affects not only the exit humidity ratio as demonstrated previously, but also the exit temperature. The effects of the sweep ratio on system performance are shown in Fig. 7. In the low sweep ratio range, the temperature falls as the sweep ratio increases, because the flow rate ratio of hot fluid (feed air) to cold fluid (sweep air) decreases. However, the increase of the sweep ratio will not bring a continuous descent of the exit temperature. As the sweep ratio increases further, the sweep air pressure drop inside the shell side will increase, thus the expansion pressure ratio of the minor turbine will decrease to ensure that the back pressure is equal to the ram air pressure. As a result, the cooling capacity produced by the minor turbine is weakened to lead to the increase of the temperature of the dehumidified air out from the membrane dehumidifier and finally the increase of the exit temperature of the system.

It can be seen also from Fig. 7 that with a required cabin temperature of 298 K, the system cooling capacity decreases monotonously as the sweep ratio increases, causing the decrease of the mass flow rate of the supply air. This means that the lower the sweep ratio is, the better the system performance is. However, the freezing risk increases because of the weakened dehumidification performance. Fig. 8 shows the

Table 2 Working conditions for simulation.

Parameter	Value
Sweep ratio φ (%)	20
Bleed air mass flow rate G_b (kg/s)	0.2
Bleed air temperature T_b (K)	490
Bleed air humidity ratio ω_b (kg/kg)	0.019
Bleed air pressure p_b (kPa)	418
Ram air mass flow rate G_r (kg/s)	0.4
Ram air temperature T_r (K)	327
Ram air humidity ratio ω_r (kg/kg)	0.019
Ram air pressure p_r (kPa)	106

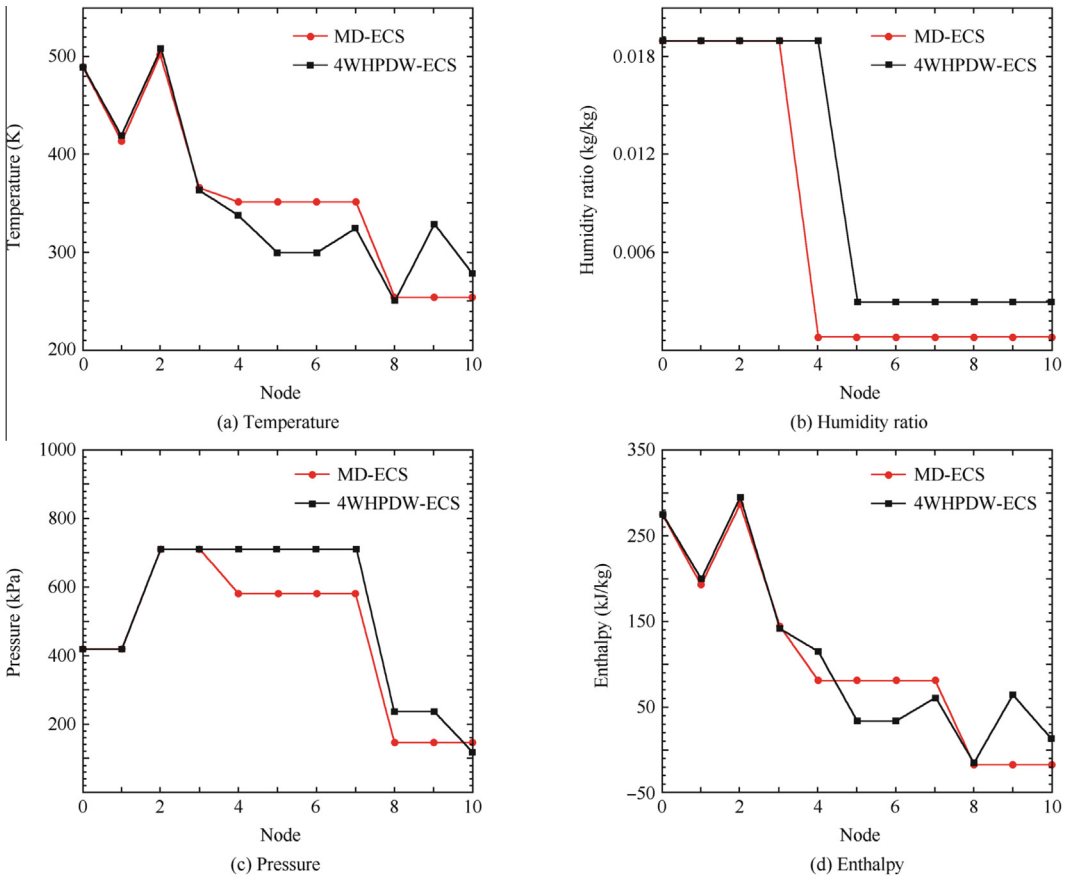

Fig. 6 Comparisons of the parameters at each node between MD-ECS and 4WHPDW-ECS.

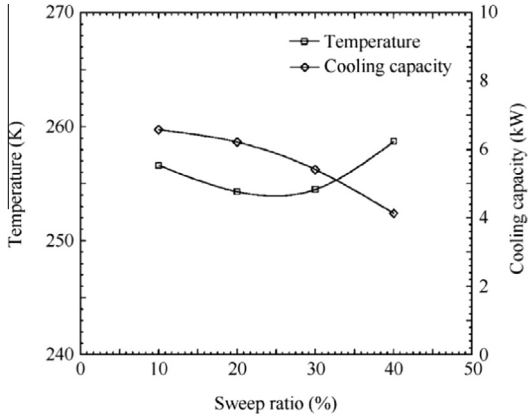

Fig. 7 Effects of sweep ratio on exit temperature and system cooling capacity.

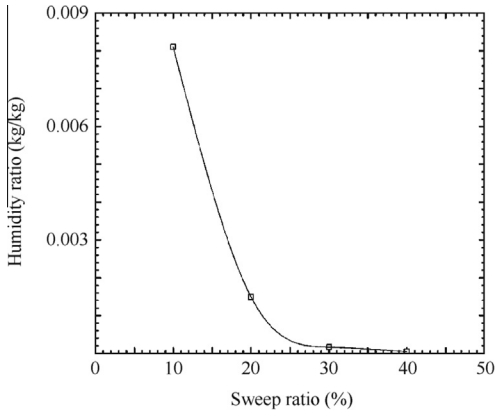

Fig. 8 Effects of sweep ratio on exit humidity ratio.

variation of the exit humidity ratio versus the sweep ratio. It is observed that the humidity ratio decreases rapidly and then tends to zero as the sweep ratio increases. We can see that the outlet humidity ratio reaches as high as 0.008 kg/kg at 10% sweep ratio, leading to a high freezing risk of the major turbine. Therefore, there should be an optimal selection for the sweep ratio. In this paper, the sweep ratio of 20% is suitable.

5. Conclusions

In this paper, a novel ECS based on membrane dehumidification (MD-ECS) is proposed and compared with the up-to-date four-wheel system (4WHPDW-ECS). Both of the two systems are modeled numerically. The simulation results indicate that the MD-ECS is theoretically feasible and has better performance. There is no phase change in the MD-ECS for water removal. The removal of water vapor is realized by the

permeation across the membrane directly in gas phase. The group of metal-made condenser and water separator applied in all the conventional high pressure de-water ECSs including the 4WHPDW-ECS is replaced by the lighter and smaller membrane dehumidifier made from polymer hollow fibers. The new system is much more efficient, much lighter and less complex. Since no phase change of water vapor occurs, the cooling capacity does not have to be consumed for condensation, but is reserved for cabin cooling. The cooling capacity of the new system is thus promoted remarkably. As the weight and performance of the ECS are finally contributed to fuel consumption, the new system realizes a lower fuel penalty compared with the 4WHPDW-ECS.

Acknowledgement

The authors appreciate the support from Aeronautical Science Foundation of China (No. 2011ZC09006).

References

1. Leo TJ, Pérez-Grande I. A thermoeconomic analysis of a commercial aircraft environmental control system. *Appl Therm Eng* 2005;**25**(2–3):309–25.
2. Vargas JVC, Bejan A. Thermodynamic optimization of finned crossflow heat exchangers for aircraft environmental control systems. *Int J Heat Fluid Flow* 2001;**22**(6):657–65.
3. Wang X, Yuan X. Reuse of condensed water to improve the performance of an air-cycle refrigeration system for transport applications. *Appl Energy* 2007;**84**(9):874–81.
4. Bejan A, Siems DL. The need for exergy analysis and thermodynamic optimization in aircraft development. *Int J Exergy* 2001;**1**(1):14–24.
5. Zhang Z, Liu S, Tian L. Thermodynamic analysis of air cycle refrigeration system for Chinese train air conditioning. *Syst Eng Procedia* 2011;**1**:16–22.
6. Zhao H, Hou Y, Zhu Y, Chen L, Chen S. Experimental study on the performance of an aircraft environmental control system. *Appl Therm Eng* 2009;**29**(16):3284–8.
7. Hamlin S, Hunt R, Tassou SA. Enhancing the performance of evaporative spray cooling in air cycle refrigeration and air conditioning technology. *Appl Therm Eng* 1998;**18**(11):1139–48.
8. Tu Y, Lin GP. Dynamic simulation of aircraft environmental control system based on flowmaster. *J Aircraft* 2011;**48**(6):2031–41.
9. Yuan W, Li Y, Wang C. Comparison study of membrane dehumidification aircraft environmental control systems. *J Aircraft* 2012;**49**(3):815–21.
10. Wu Y, Peng X, Liu J, Kong Q, Shi B, Tong M. Study on the integrated membrane processes of dehumidification of compressed air and vapor permeation processes. *J Membr Sci* 2002;**196**(2):179–83.
11. Bolto B, Hoang M, Xie Z. A review of water recovery by vapour permeation through membranes. *Water Res* 2012;**46**(2):259–66.
12. Fan H, Peng Y. Application of PVDF membranes in desalination and comparison of the VMD and DCMD processes. *Chem Eng Sci* 2012;**79**:94–102.
13. Ito A. Dehumidification of air by a hygroscopic liquid membrane supported on surface of a hydrophobic microporous membrane. *J Membr Sci* 2000;**175**(1):35–42.
14. Zhang LZ. Coupled heat and mass transfer through asymmetric porous membranes with finger-like macrovoids structure. *Int J Heat Mass Transfer* 2009;**52**(3–4):751–9.
15. Zhang LZ. A fractal model for gas permeation through porous membranes. *Int J Heat Mass Transfer* 2008;**51**(21–22):5288–95.
16. Zhang LZ. Heat and mass transfer in a randomly packed hollow fiber membrane module: a fractal model approach. *Int J Heat Mass Transfer* 2011;**54**(13):2921–31.
17. Zhang LZ. An analytical solution to heat and mass transfer in hollow fiber membrane contactors for liquid desiccant air dehumidification. *J Heat Transfer* 2011;**133**(9):092001.
18. Wickramasinghe SR, Han B. Designing microporous hollow fibre blood oxygenators. *Chem Eng Res Des* 2005;**83**(3):256–67.
19. Wu J, Chen V. Shell-side mass transfer performance of randomly packed hollow fiber modules. *J Membr Sci* 2000;**172**(1–2):59–74.
20. Viegas RMC, Rodrıguez M, Luque S, Alvarez JR, Coelhoso IM, Crespo JPSG. Mass transfer correlations in membrane extraction: analysis of Wilson-plot methodology. *J Membr Sci* 1998;**145**(1):129–42.
21. Zhang LZ. An analytical solution for heat mass transfer in a hollow fiber membrane based air-to-air heat mass exchanger. *J Membr Sci* 2010;**360**(1–2):217–25.
22. Zhang LZ, Huang SM. Coupled heat and mass transfer in a counter flow hollow fiber membrane module for air humidification. *Int J Heat Mass Transfer* 2011;**54**(5–6):1055–63.
23. Lipnizki F, Field RW. Mass transfer performance for hollow fibre modules with shell-side axial feed flow: using an engineering approach to develop a framework. *J Membr Sci* 2001;**193**(2):195–208.
24. Juang R, Lin S, Yang M. Mass transfer analysis on air stripping of VOCs from water in microporous hollow fibers. *J Membr Sci* 2005;**255**(1–2):79–87.

Yuan Weixing received the Ph.D. in 1995 in the Department of Man-Machine-Environment Engineering, School of Aeronautic Science and Engineering, Beihang University, Beijing, China. He is now an associate professor at Beihang University. His main research interests include solar energy, heat pumps, micro-climate cooling, and environmental control in aircraft and spacecraft.